metals

MDPI

Article

Textures of Non-Oriented Electrical Steel Sheets Produced by Skew Cold Rolling and Annealing

Youliang He [1,*] and Erik J. Hilinski [2]

[1] CanmetMATERIALS, Natural Resources Canada, Hamilton, ON L8P 0A5, Canada
[2] Tempel Steel Co., Chicago, IL 60660, USA; ehilinski@tempel.com
* Correspondence: youliang.he@canada.ca

Abstract: In order to investigate the effect of cold rolling deformation mode and initial texture on the final textures of non-oriented electrical steels, a special rolling technique, i.e., skew rolling, was utilized to cold reduce steels. This not only altered initial textures but also changed the rolling deformation mode from plane-strain compression (2D) to a more complicated 3D mode consisting of thickness reduction, strip elongation, strip width spread and bending. This 3D deformation induced significantly different cold-rolling textures from those observed with conventional rolling, especially for steels containing low (0.88 wt%) and medium (1.83 wt%) amounts of silicon at high skew angles (30° and 45°). The difference in cold-rolling texture was attributed to the change of initial texture and the high shear strain resulting from skew rolling. After annealing, significantly different recrystallization textures also formed, which did not show continuous <110>//RD (rolling direction) and <111>//ND (normal direction) fibers as commonly observed in conventionally rolled and annealed steels. At some skew angles (e.g., 15–30°), the desired <001>//ND texture was largely enhanced, while at other angles (e.g., 45°), this fiber was essentially unchanged. The formation mechanisms of the cold rolling and recrystallization textures were qualitatively discussed.

Keywords: non-oriented electrical steel; texture; rolling; X-ray diffraction; recrystallization; thermomechanical processing

Citation: He, Y.; Hilinski, E.J. Textures of Non-Oriented Electrical Steel Sheets Produced by Skew Cold Rolling and Annealing. *Metals* **2022**, *12*, 17. https://doi.org/10.3390/met12010017

Academic Editor: Andrey Belyakov

Received: 12 November 2021
Accepted: 20 December 2021
Published: 22 December 2021

1. Introduction

Non-oriented electrical steels (NOES) are commonly used as soft magnetic lamination material in the manufacture of cores for electric motors. The silicon content of the alloy, the cleanliness of the steel, the thickness of the lamination and the microstructure and texture of the steel sheets, etc., determine the magnetic quality of the final laminated core and significantly affect the electric motor's energy efficiency. Improving the magnetic properties of NOES through the optimization of crystallographic texture has been a field of extensive research for many years [1–10]. Although numerous papers have documented improvement in crystallographic textures (and, thus, the magnetic properties) of electrical steels by varying operational parameters during hot rolling, cold rolling, annealing or through annealing after hot rolling (hot band annealing) [11–14] or annealing between cold rolling passes (intermediate annealing) [14–16], the final textures obtained using these techniques are still not ideal. The results usually showed a weakening of the magnetically unfavorable <111>//ND (γ-fiber) texture, sometimes accompanied by a slight to moderate strengthening of the desired <001>//ND (θ-fiber) texture. The orientation state is still far from the perfect {001} texture with the easy <100> directions uniformly distributed in all directions of the steel sheet, as required for optimal magnetization in rotating machines [2].

It has been shown in numerous studies [17–20] that body-centered-cubic (bcc) metals after conventional hot rolling, cold rolling and final annealing usually show a similar texture, mainly consisting of an α-fiber (<110>//RD) and a γ-fiber, even though the chemical compositions and processing parameters have been widely varied. The evolution of texture in electrical steels from a cast slab to final cold-rolled and annealed sheets is a complicated

process where the original crystal orientations created in solidification are subjected to a series of changes due to deformation, recrystallization and phase transformation (phase transformation only occurs in electrical steels with relatively low silicon contents [21,22]) during subsequent hot rolling, cold rolling and annealing processes. In conventional plate and sheet rolling, the same deformation mode (plane-strain compression) coupled with essentially the same active slip systems in bcc metals usually results in similar deformation textures, although the differences in initial texture and the amount of reduction may result in some variations in final texture. In conventional rolling practices, the rolling directions between hot rolling and cold rolling, or between rolling passes (in reversing rolling), may be changed to achieve a good control of the flatness and gauge of the final sheets. However, these changes in rolling direction (180° rotation around ND) essentially do not change texture or microstructure due to the orthorhombic symmetry associated with the rolling process. Thus, it is not considered as a method for changing the texture of the material. In order to significantly alter rolling texture and, thus, change the final annealing texture, the initial texture or the deformation mode, or both, must be changed.

A well-known rolling technique that alters initial texture is *cross rolling*, where the texture after hot rolling is rotated 90° about the ND during cold rolling, which has been shown to be very effective in producing the desired {001} texture in electrical steels [2,23]. *Inclined rolling* [5,24], where the initial texture is rotated around the ND by an angle between 0° and 90°, is also an effective method for changing the initial texture and improving the final texture. *Asymmetric rolling* is a special rolling technology that changes the deformation mode from plane-strain compression to shear, which also results in significant changes in texture [25]. *Skew rolling* [26] is yet another special rolling process where both the initial texture and the deformation mode are simultaneously altered by simply feeding the steel plate into roll bites at an angle (ω) between 0° and 45° from the conventional hot rolling direction (HRD). It has been shown [26] that skew rolling processes can significantly change the cold rolling textures of electrical steels. However, the textures after final annealing have not been investigated. This paper presents the evolution of macrotextures of electrical steels from hot band annealing to skew cold rolling and final annealing by evaluating the volume fractions of common texture fibers and components. Three NOES grades containing various amounts of silicon (weight percentage), i.e., 0.88%, 1.83% and 2.77%, were investigated. The textures were characterized via X-ray Diffraction (XRD) on the mid-thickness plane of the steel sheets. The effect of skew cold rolling angle on the volume fractions of typical texture fibers and components, e.g., α-fiber (<110>//RD), γ-fiber (<111>//ND), θ-fiber (<001>//ND) and Goss ({011}<100>), in the cold rolled and final annealed steel sheets is discussed.

2. Materials and Methods

The chemical compositions of the NOES (A, B and C) investigated in this study are listed in Table 1. The steels were vacuum melted and cast into ingots of 200 mm × 200 mm (cross section). The ingots were first reheated to ~1040 °C and hot rolled to intermediate plates of ~25 mm (87.5% thickness reduction). After removing the oxides on the surfaces, the plates were reheated again to ~1040 °C and hot rolled to bands about 2.2~2.6 mm thick (88–86% reduction). The hot bands were then pickled in hot HCl acid and annealed at ~840 °C for 60 h in a 100% dry H_2 atmosphere.

Table 1. Chemical compositions of the studied non-oriented electrical steels (wt%).

Steel	C	Mn	P	S	Si	Al	Fe
A	0.0021	0.307	0.010	0.0011	0.875	0.461	Bal.
B	0.0023	0.299	0.010	0.0011	1.826	0.515	Bal.
C	0.0033	0.303	0.010	0.0011	2.767	0.516	Bal.

The hot-rolled and annealed bands were cut into rectangular samples (200 mm × 50 mm) along the HRD (Figure 1a) and cold rolled using a skew rolling scheme (Figure 1b) as de-

tailed in [26]. Five skew angles (ω = 0°, 15°, 22.5°, 30° and 45°) and two feeding patterns (Figure 1c) were employed in the skew cold rolling process, which produced a total of (5 × 2 × 3) − 3 = 27 samples (when ω = 0°, the two feeding patterns are identical and, thus, not repeated). The details of the samples are listed in Table 2.

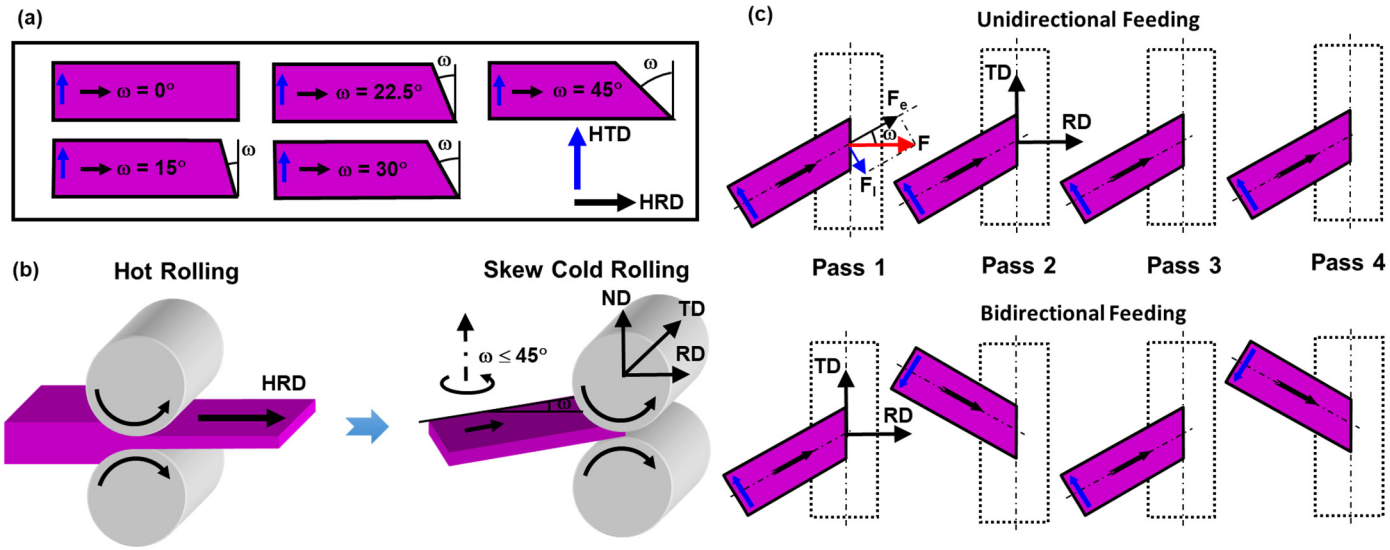

Figure 1. Schematic illustration of the skew cold rolling process [26]: (**a**) sample cutting from hot rolled plate, (**b**) the skew rolling process and (**c**) the two feeding patterns. HRD: hot rolling direction; HTD: hot transverse direction.

Table 2. Sheet thicknesses after skew cold rolling.

Steel A (0.88 wt% Si)		Steel B (1.83 wt% Si)		Steel C (2.77 wt% Si)	
Sample ID	**Thickness (mm)**	**Sample ID**	**Thickness (mm)**	**Sample ID**	**Thickness (mm)**
A-0	0.538	B-0	0.540	C-0	0.552
A-15-Unidirect	0.543	B-15-Unidirect	0.524	C-15-Unidirect	0.590
A-15-Bidirect	0.505	B-15-Bidirect	0.520	C-15-Bidirect	0.570
A-22.5-Unidirect	0.543	B-22.5-Unidirect	0.556	C-22.5-Unidirect	0.603
A-22.5-Bidirect	0.540	B-22.5-Bidirect	0.532	C-22.5-Bidirect	0.582
A-30-Unidirect	0.508	B-30-Unidirect	0.570	C-30-Unidirect	0.584
A-30-Bidirect	0.540	B-30-Bidirect	0.534	C-30-Bidirect	0.588
A-45-Unidirect	0.563	B-45-Unidirect	0.583	C-45-Unidirect	0.636
A-45-Bidirect	0.544	B-45-Bidirect	0.607	C-45-Bidirect	0.692

The variation in feeding angle not only altered the initial texture of the steel but also changed the deformation mode from plane-strain compression (2D) to a complicated three-dimensional (3D) mode comprising a combination of thickness reduction, strip elongation, strip width spread and bending [26]. As shown in Figure 1c, the frictional force **F** (perpendicular to the rolls, along the RD) generated between the rolls and the material can be decomposed into two components: one in the HRD ($F_e = F \cdot \cos\omega$) and the other along the HTD ($F_l = F \cdot \sin\omega$). The force in HRD elongates the material, while the force along the HTD causes width spread and bending of the material. Apparently, the deformation of the material in skew rolling is significantly different from conventional rolling (plane-strain compression), since the width spread and in-plane bending are not observed in conventional rolling. The complicated 3D deformation mode of skew rolling is expected to significantly change the nature of the deformation as well as the orientation flow and crystallographic texture.

Due to the changes in rolling direction and initial texture, the thicknesses of the final strips produced with different skew angles under the same operational parameters

(i.e., number of passes and reduction rate per pass) vary considerably. Finite element analysis of the skew rolling process has shown [26] that the normal stress in the thickness direction decreases with an increase in skew angle (when the angle is greater than 15°); thus, generally the larger the skew angle, the smaller the stress in the normal direction and the larger the thickness. On the other hand, due to the anisotropy of the initial material, the change of the initial texture changes the material properties in certain directions, which also causes differences in springback after deformation. As a result, the final thickness of the sheet may be different even if the roll gap is set to the same size during rolling. Furthermore, the increase in Si content in the steel results in an increase in yield strength [26]. A material with a higher yield strength has a greater ratio of elastic-to-plastic strain and exhibits larger springback. Thus, steel with a higher amount of Si generally has a larger final thickness.

After skew cold rolling, the steel sheets were annealed at different temperatures (800, 920 and 1035 °C for Steels A, B and C, respectively) for 30 s. Annealing temperatures were determined according to the Si and Al contents based on an empirical equation provided in [27]. For Steels A and B, since Si contents are relatively low and the materials have phase transformation, the annealing temperatures determined according to the equation are higher than the recrystallization temperatures but lower than phase transformation temperatures [24]. This can ensure that the annealing is conducted in the ferrite region to eliminate the effect of phase transformation on the texture. For Steel C, due to the high Si content, there is no phase transformation in the steel; thus, even with a high annealing temperature, recrystallization occurs in the ferrite phase. Annealing was conducted in an argon-protected environment with a heating rate of 720 °C/h and a holding time of 30 s at the designated annealing temperatures for all samples. The relatively slow heating rate was selected to simulate batch anneal conditions in industry, where due to the large coil, the temperature of steel increases slowly. The samples were finally furnace cooled to room temperature.

The textures of the steel sheets after hot band annealing, skew cold rolling and final annealing were measured via XRD using a Bruker D8 Discover with Co K-α X-ray radiation on the mid-thickness planes of the sheets. All texture measurements were referred to the final strips' length, width and thickness directions. Orientation density functions (ODF's) were calculated from three measured incomplete pole figures, (110), (211) and (200), using the MTEX software [28] using Bunge's Euler angles. Due to the novel positioning of the plate with respect to cold mill rolls and the asymmetric forces applied to the material, orthorhombic sample symmetry does not apply to the skew rolling process [26]. Thus, ODFs' were calculated using triclinic sample symmetry, and the textures are plotted in sections with φ_1 = 0°–360° instead of the familiar 0°–90° (for conventional rolling with orthorhombic sample symmetry). For calculation of the volume fractions of texture fibers and components, a tolerance angle of 10° was used to include all orientations within this angle (deviation from the ideal orientations).

3. Results

3.1. Textures before Skew Cold Rolling

As shown in [26], the skew rolling process alters the initial texture before cold rolling by feeding the hot-rolled band at an angle (ω) relative to the conventional cold rolling direction (Figure 1b,c). As a result, the initial texture with respect to RD, TD and ND is rotated by ω around the ND from the hot-rolled band. The resulting textures at various skew angles for the three steels (after hot rolling and annealing) are shown in Figure 2. The variation in volume fractions of the major texture fibers and the rotated cube component ({001}<110>) is illustrated in Figure 3.

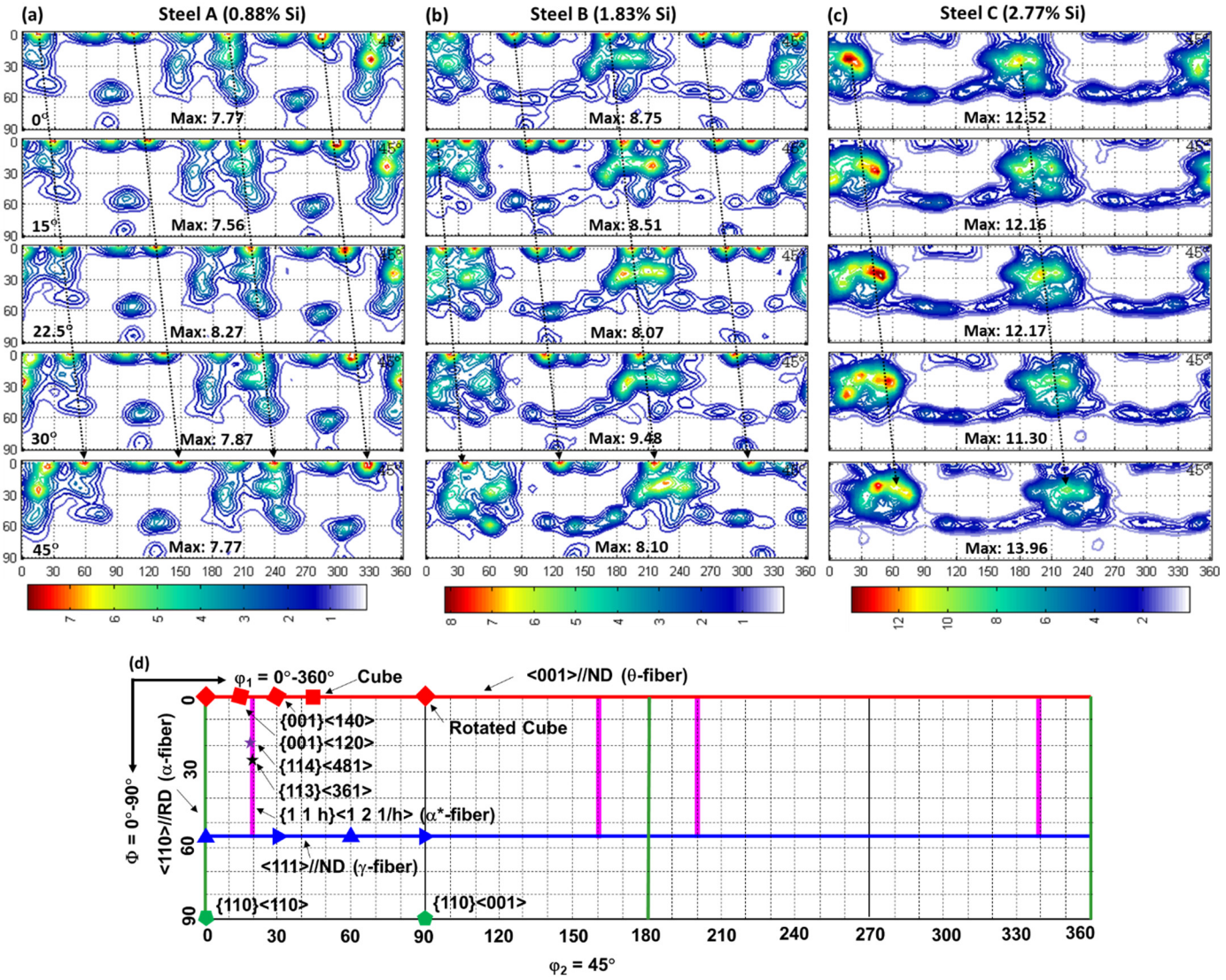

Figure 2. Initial textures before skew cold rolling (rotation of the texture): (**a**) Steel A, (**b**) Steel B, (**c**) Steel C and (**d**) index of the major texture components and fibers. φ_2 = 45° ODF sections in Bunge–Euler angles.

For conventional rolling (ω = 0°), the texture of Steel A (0.88 wt% Si) is dominated by components on the <100>//ND fiber, and there is no continuous γ-fiber or α-fiber and only with some discrete components on these fibers (Figure 2a). With the increase in silicon content, the maximum texture intensity of the steel increases, and the α-fiber is strengthened (Figure 3a), while the θ-fiber is weakened (Figure 3c). The rotated cube component ({001}<110>) shows a different trend (Figure 3d), i.e., both low and high silicon steels (Steels A and C) have a small volume fraction, while the medium silicon steel (Steel B) illustrates a relatively large volume fraction. It should be noted that the steel with 2.77% Si (Steel C) illustrates a significantly different texture from the other steels, i.e., showing a very strong {113}<361> component on the α*-fiber ({1 1 h}<1 2 1/h>) (Figure 2c) and a stronger γ-fiber than compared to the other two steels (Figure 3b). This is mainly caused by the difference in Si content in the steels: the steels with low silicon concentrations (Steels A and B) might have undergone phase transformation during hot rolling, while the high silicon steel (Steel C) does not have phase transformation.

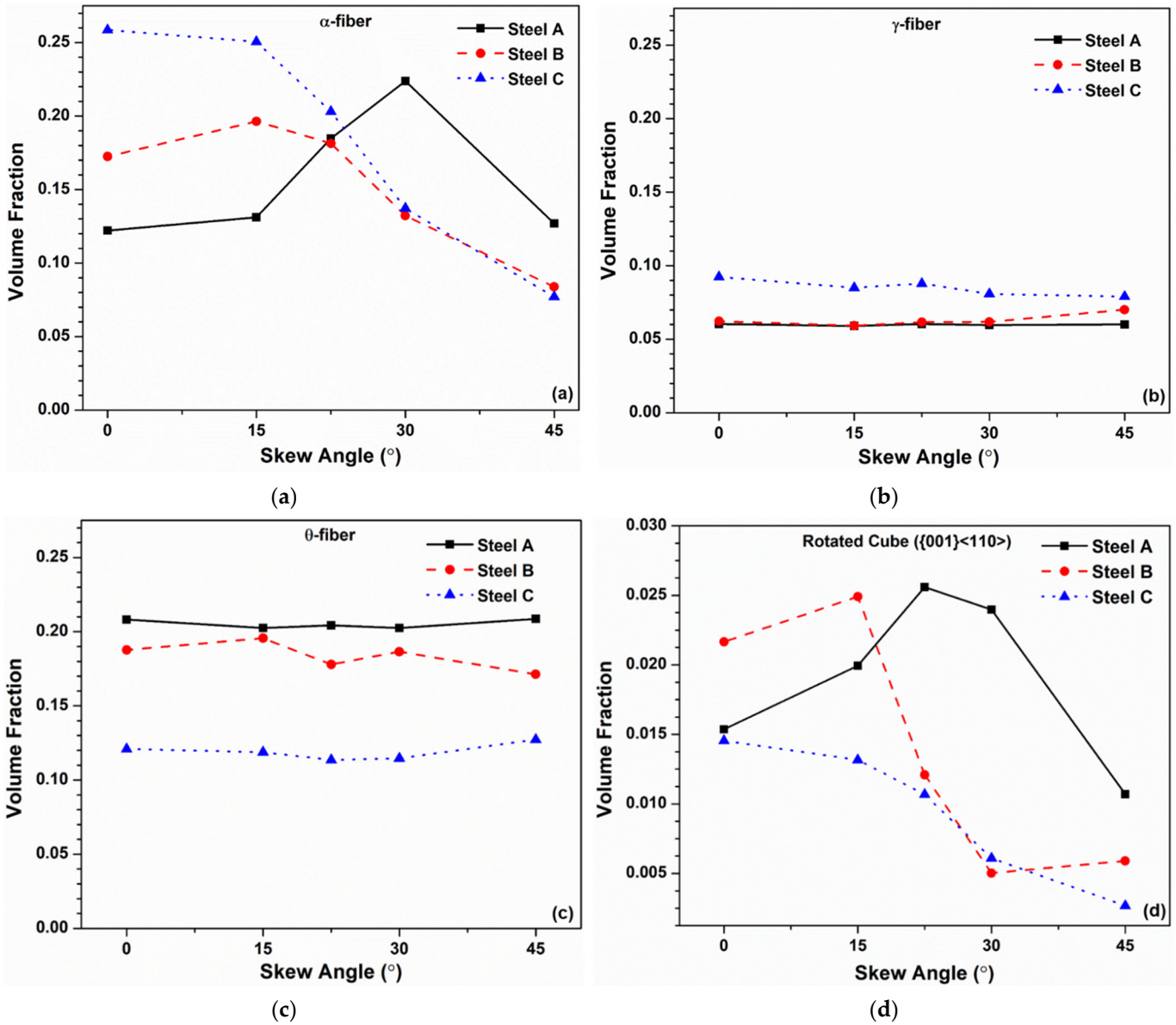

Figure 3. Variations of the volume fractions of typical texture fibers: (**a**) α-fiber, (**b**) γ-fiber, (**c**) θ-fiber and the rotated cube component (**d**), with respect to the rotation around the ND.

Since the rotation during skew rolling is around the ND, crystal planes parallel to the steel sheet are not changed, but the crystal directions within these planes are rotated. As a result, orientations on the <100>//ND and <111>//ND fibers are moved along the same fibers, i.e., the φ_1 angle changes (see arrows in Figure 2). Thus, the volume fractions of these fibers only show slight fluctuations when rotated around ND (Figure 3b,c). However, it should be noted that although the rotation essentially does not change the volume fractions of these fibers, the major texture components on these fibers are shifted because of the rotation. For example, for Steel A, the strong {001}<1$\bar{2}$0> component on the θ-fiber after conventional rolling (ω = 0°) was shifted to {001}<1$\bar{4}$0>, {001}<100> (Cube) and {001}<$\overline{14}$0> when the skew angle was 15°, 30° and 45°, respectively. Each rotation may strengthen some components on this fiber while weakening other components at the same time (the overall volume fraction of the fiber essentially does not change). For example, the rotated cube ({001}<110>) component of all three steels experiences large variations due to the rotation (Figure 3d).

On the other hand, since the α-fiber is composed of orientations with a series of planes ({111}, {112}, {113}, etc.) sharing the same <110> direction ($\varphi_1 = 0°$), the rotation around ND changes this fiber (φ_1 is changed) to other orientations, resulting in large variations in the volume fraction of this fiber (Figure 3a). Similarly, the α*-fiber (with $\varphi_1 \approx 20°$) is parallel to the α-fiber, which is also changed by rotating around ND. As observed in Figure 2c, the strong {113}<361> component (on the α*-fiber) gradually shifted from $\varphi_1 \approx 20°$ to $\varphi_1 \approx 65°$ when the rotation angle gradually increased.

3.2. Textures after Skew Cold Rolling

3.2.1. Unidirectional Feeding

The textures after skew cold rolling under *unidirectional feeding* are shown in Figure 4. With most of the skew angles, the deformation textures are still very similar to typical bcc textures after conventional rolling, i.e., mainly consisting of an α-fiber and a γ-fiber. However, the textures of Steels A and B after skew rolling at ω = 45° show significantly different textures: First, the maximum texture intensities (31.55 and 38.04, respectively) at this angle are much higher than those (11.64–13.64 and 15.56–18.35, respectively) at other angles; second, the texture is dominated by a θ-fiber component ({001}<140>) and not the rotated cube or {112}<110>/{223}<110> components as observed with other angles. The texture of Steel C differs considerably from Steels A and B in the following ways: (i) the maximum texture intensity (29.83) is observed at ω = 15° instead of 45°; (ii) the strongest texture component is usually on the α-fiber ({112}<110>/{223}<110>) and not on the θ-fiber. Nevertheless, at ω = 45°, the strongest texture component ({001}<120>) in Steel C is also on the θ-fiber, which is similar to the other two steels.

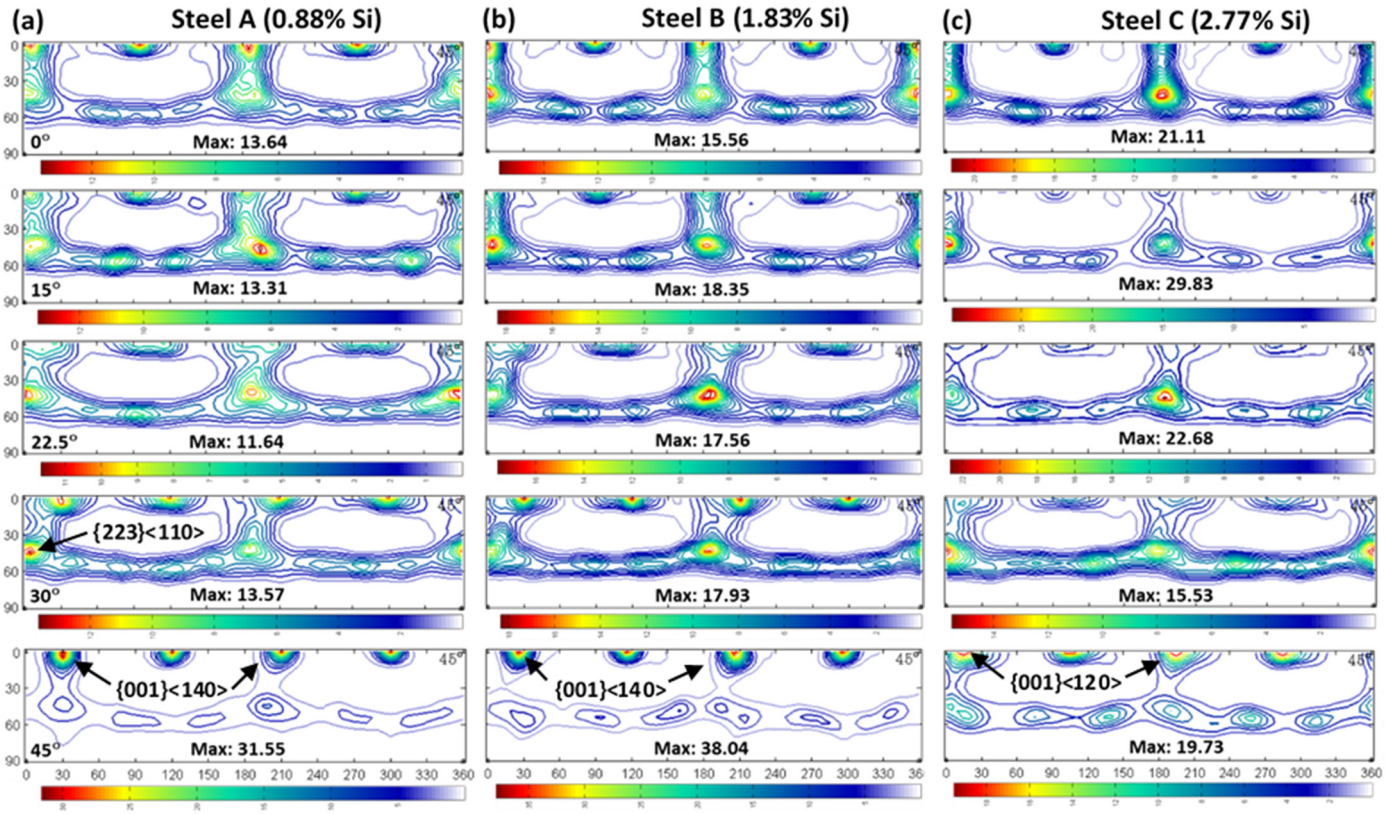

Figure 4. Textures after skew cold rolling with unidirectional feeding [26]: (**a**) Steel A, (**b**) Steel B and (**c**) Steel C.

The variation in the volume fractions of the common texture fibers and rotated cube component with respect to the skew angle is shown in Figure 5. With an increase in the

skew angle, the α-fiber of all the three steels only shows very small variations. The only apparent increase in the α-fiber is observed in Steel C when ω = 45°. In the other two steels, the α-fiber slightly decreases with the skew angle. The γ-fiber also only shows small variations with respect to the skew angle. However, the γ-fiber is strengthened slightly for all three steels when the skew angle is 15°–30°. It is also noted that the volume fraction of the γ-fiber in Steel C is apparently higher than those of Steels A and B, similar to those before cold rolling. The most significant effect of skew rolling is on the θ-fiber. It is observed that for all three steels, with the increase in skew angle, the volume fraction of the θ-fiber gradually increases, especially when the skew angle is greater than 22.5°. At a skew angle of 45°, Steel B shows an extremely large fraction (~46%) of θ-fiber, while those of the other two steels also reach ~38%.

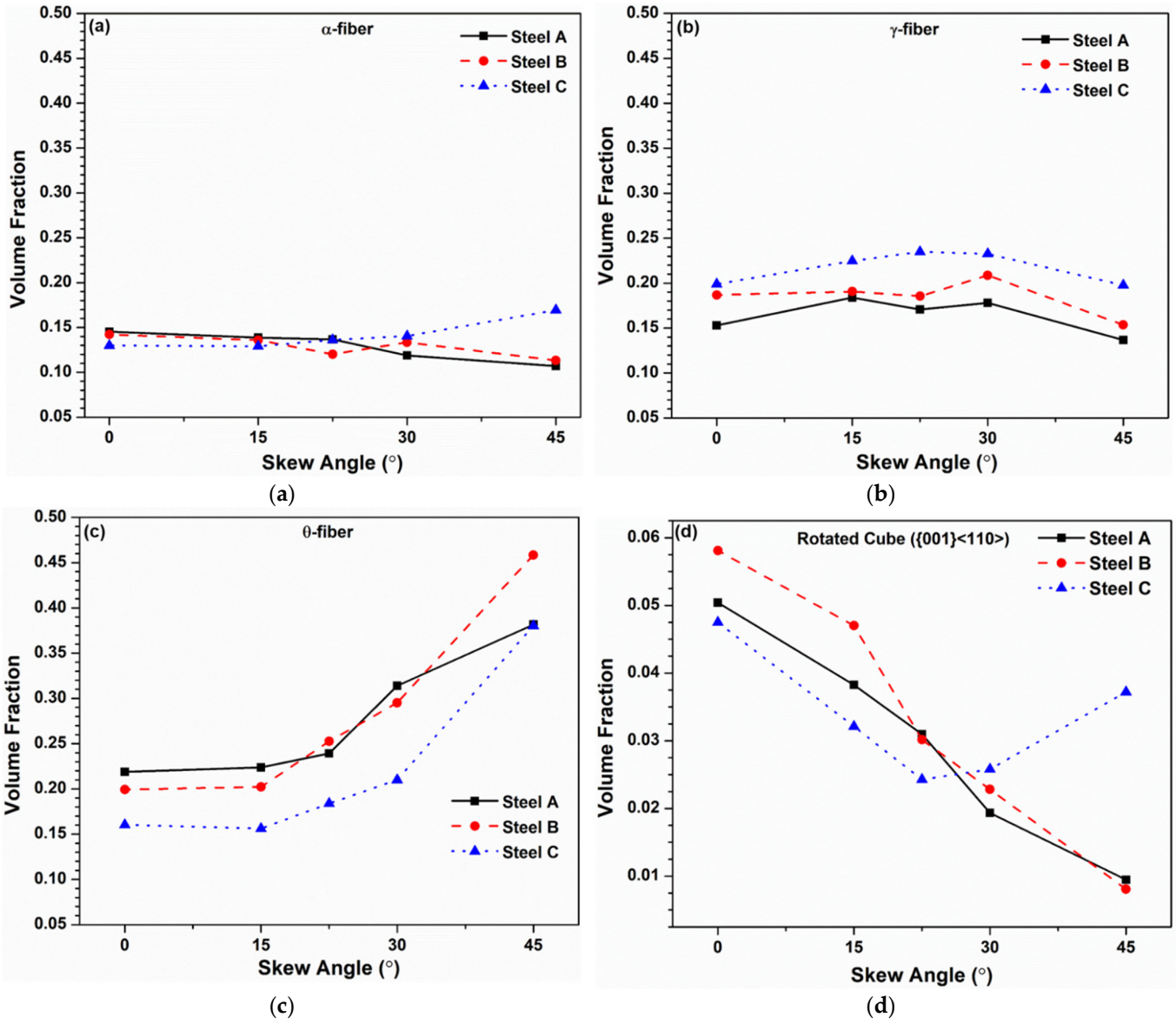

Figure 5. Comparison of the volume fractions of common texture fibers, (**a**) α-fiber, (**b**) γ-fiber, (**c**) θ-fiber and the rotated cube component (**d**), after skew cold rolling under unidirectional feeding.

The effect of skew rolling on the rotated cube component (on the θ-fiber) is also large. For Steels A and B, with the increase in skew angle, the volume fraction of the rotated cube almost linearly decreases, while for Steel C it decreases until 22.5° and starts to increase with skew angles $\omega \geq 30°$ (Figure 5d). Compared to the as-hot-band-annealed textures

shown in Figure 3d, it is observed that the volume fraction of the rotated cube component generally increased after skew rolling for all three steels at most skew angles as evidenced by the difference in scale in Figures 3 and 5 (the exception being Steel A at 30° and 45°, which shows a slight decrease). The volume fraction of the rotated cube component of Steel C after skew rolling at 45° increased by ~13 times.

To summarize, compared to conventional rolling (ω = 0°), skew rolling generally enhances θ-fiber texture while only slightly impacting the α-fibers and γ- fibers. At a skew angle of ω = 45°, the θ-fiber texture volume fraction is 1.7, 2.3 and 2.4 times of that after conventional rolling for Steels A, B and C, respectively, while the γ-fiber is slightly weakened or unchanged.

3.2.2. Bidirectional Feeding

The textures after skew-cold rolling with *bidirectional feeding* are shown in Figure 6. Again, in most cases, the textures are similar to those from conventional rolling, i.e., with α-fibers and γ-fibers as the main textures. When the skew angle is 45°, there is also a strong θ-fiber component in each of the steels, with Steel A having an extremely high texture intensity of 48.67, about 2–4 times those at other skew angles. The strongest component is {001}<$\bar{1}$40> for Steels A and C and {001}<1$\bar{4}$0> for Steel B. Compared to Steel A (which has the lowest silicon content), the maximum texture intensities of Steels B and C (which contain higher amounts of silicon than Steel A) are much lower, i.e., less than half of Steel A. In addition, the γ-fibers in these two steels are continuous, while in Steel A there are only weak discrete components on the γ-fiber.

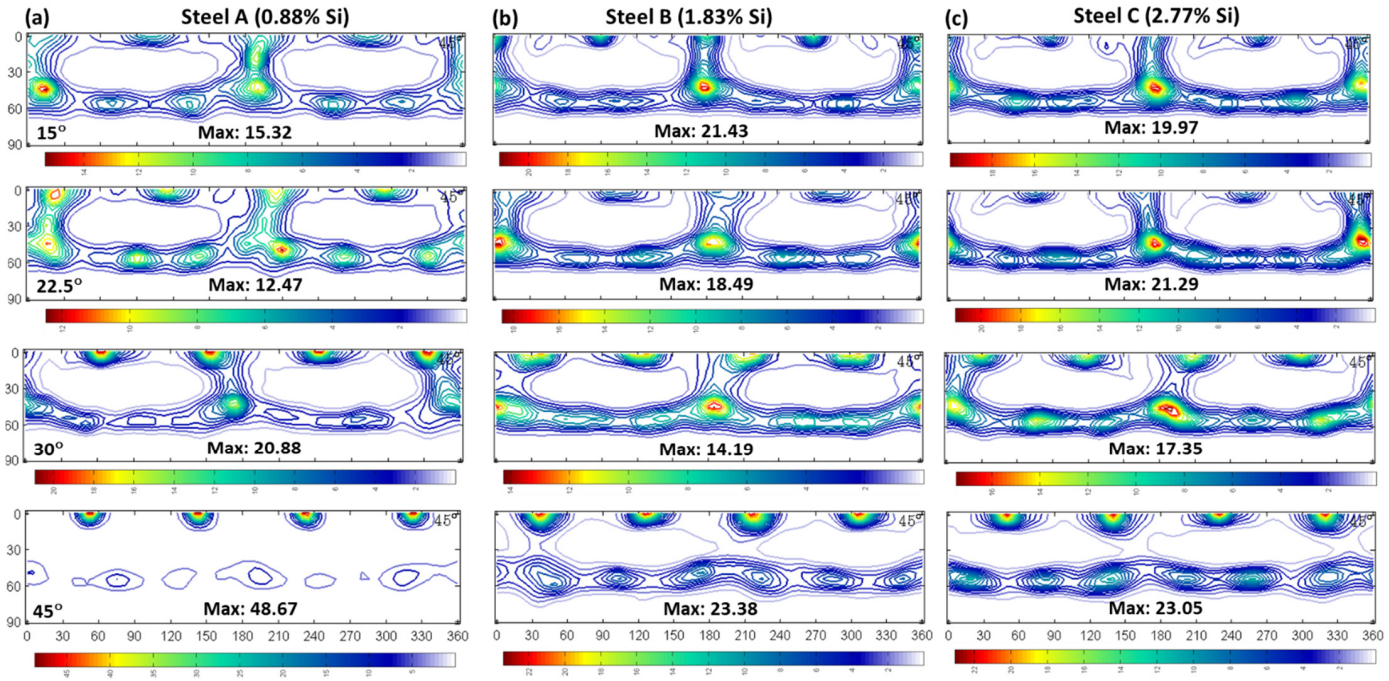

Figure 6. Textures after skew cold rolling with bidirectional feeding [26]: (**a**) Steel A, (**b**) Steel B and (**c**) Steel C.

The variations of the common texture fibers and components (Figure 7) are very similar to those from unidirectional feeding, i.e., the α-fiber and γ-fiber only show slight variations with respect to the skew angle, while the θ-fiber volume fraction increases significantly with the increase in skew angle. Again, the maximum volume fractions (ω = 45°) of the θ-fiber of Steels A, B, and C reach 50.4%, 37.6% and 38.2%, respectively. However, it is noted that the volume fraction of the rotated cube component of Steel C does not increase (monotonic decrease) when ω ≥ 30°, which is different from the *unidirectional feeding* case. Apparently, from a texture point of view, skew rolling with either unidirectional or bidirectional feeding

generally produces similar deformation textures, although the maximum texture intensities and some individual texture components do show discrepancies.

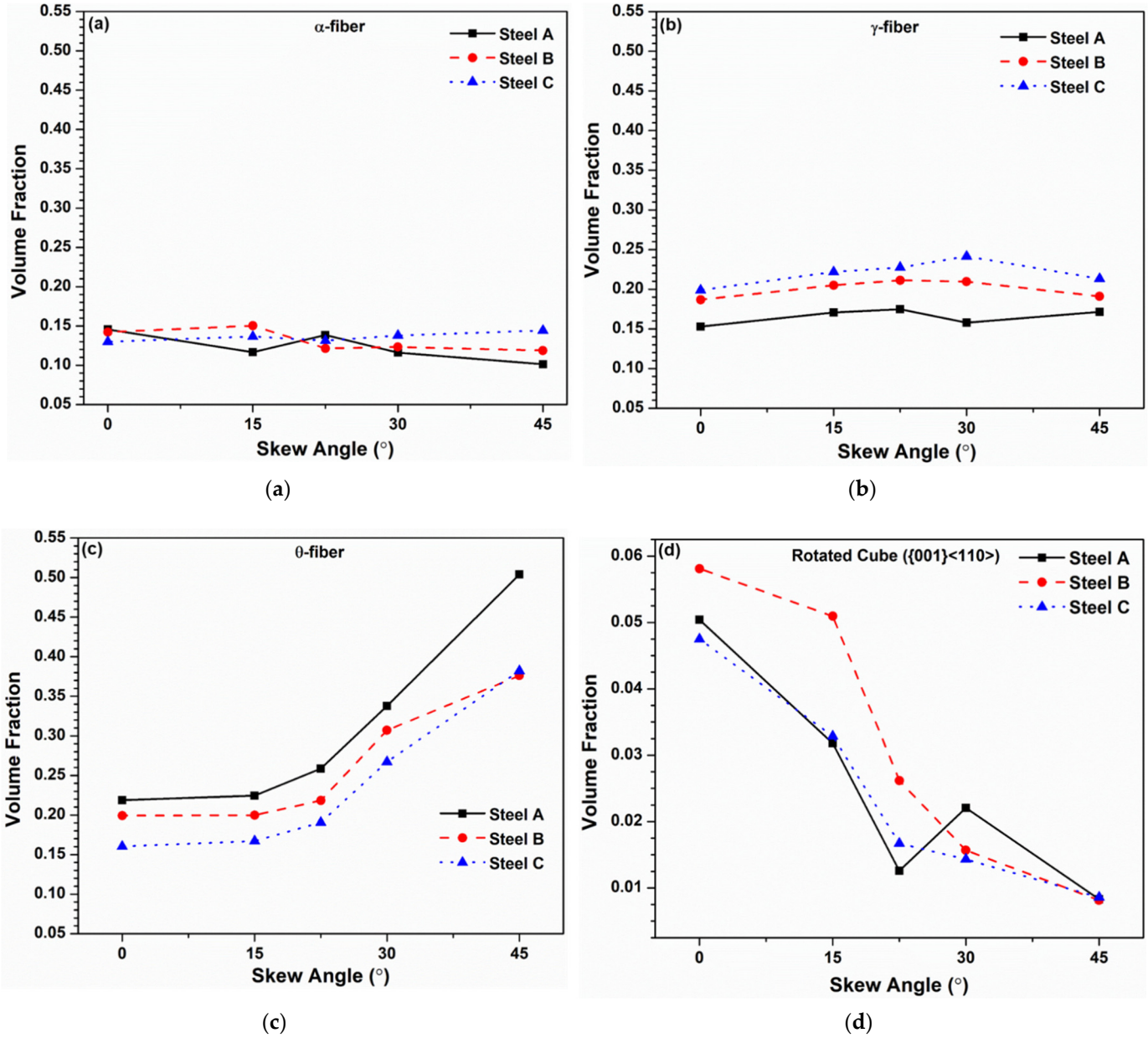

Figure 7. Comparison of the volume fractions of common texture fibers, (**a**) α-fiber, (**b**) γ-fiber, (**c**) θ-fiber and the rotated cube component (**d**), after skew cold rolling with bidirectional feeding.

3.3. Textures after Annealing

3.3.1. Unidirectional Feeding

The ODFs of the skew-cold-rolled steels after annealing are shown in Figure 8. The variations in volume fractions of the typical texture fibers and the Goss component are illustrated in Figure 9. Compared to those after cold rolling (Figure 4), the maximum texture intensities are largely reduced after recrystallization and usually the higher the initial intensity after cold rolling, the lower the final intensity after recrystallization. Similarly to those after cold rolling, normally the higher the silicon content, the larger the maximum texture intensity after annealing.

For the 0.88% Si steel, the annealing texture after conventional rolling ($\omega = 0°$) consists of strong components near the cube and Goss (Figure 8a) orientations, which are the desired

textures for NOES. As a result, the θ-fiber (Figure 9a) and Goss (Figure 9d) volume fractions in this steel are high. In addition, the magnetically unfavorable γ-fiber texture is very weak (Figures 8a and 9b). Thus, for low silicon NOES, conventional rolling is able to produce the desired final textures. With conventional rolling, if the silicon content is increased to 1.83% and 2.77%, both the α-fibers and γ-fibers are enhanced, while the θ-fiber is weakened. On the other hand, the Goss volume fraction is significantly reduced (Figure 9d).

After skew cold rolling at a 15° angle, the volume fractions of the α-fibers and γ- fibers of the 1.83% and 2.77% Si steels are slightly reduced, while that of the θ-fiber considerably increased. For both steels, the Goss volume fraction essentially does not change. The 0.88% Si steel behaves differently from these two steels, i.e., the volume fraction of the α-fiber essentially does not change, while that of the γ-fiber increases considerably. The volume fraction of the θ-fiber increases slightly, while that of the Goss component decreases significantly from 3.2% to 1.6%.

When the skew rolling angle was 22.5°, the α-fiber volume fractions of the 0.88% and 1.83% Si steels slightly increased, while that of the 2.77% Si steel decreased. The volume fraction of the γ-fiber shows different trends. While that of the 2.77% Si steel displays a large jump (because of an extremely strong near γ-fiber component with an intensity of 28.22), those of 0.88% and 1.83% Si steels essentially did not change. The θ-fiber volume fraction continues to increase for both the 1.83% and 2.77% Si steels, while that of the 0.88% Si steel plateaus. The Goss volume fraction of the 1.83% Si steel increases, while those of the 0.88% and 2.77% Si steels decrease.

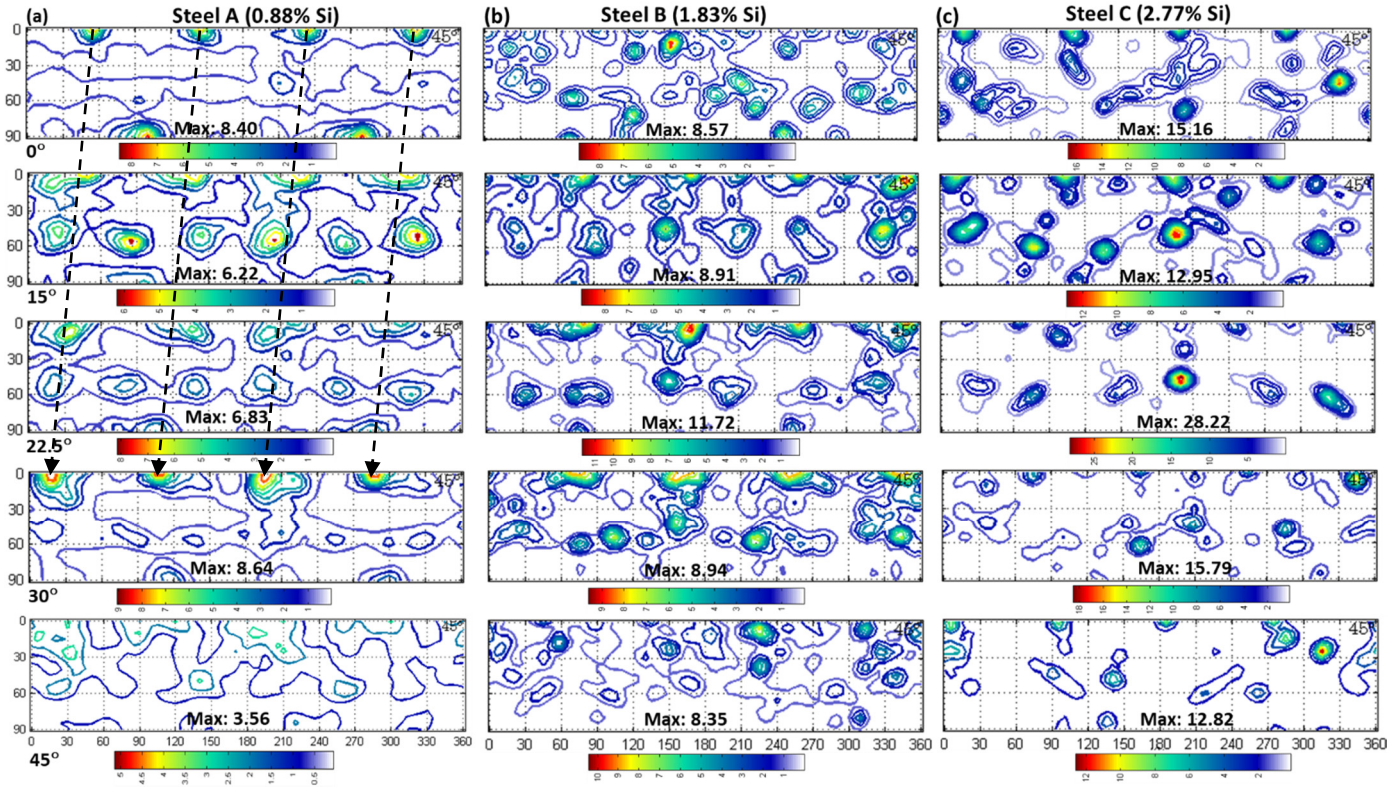

Figure 8. Textures of the skew-cold-rolled steels (unidirectional feeding) after annealing: (**a**) Steel A, (**b**) Steel B and (**c**) Steel C. $\varphi_2 = 45°$ sections of the Euler space (Bunge notation).

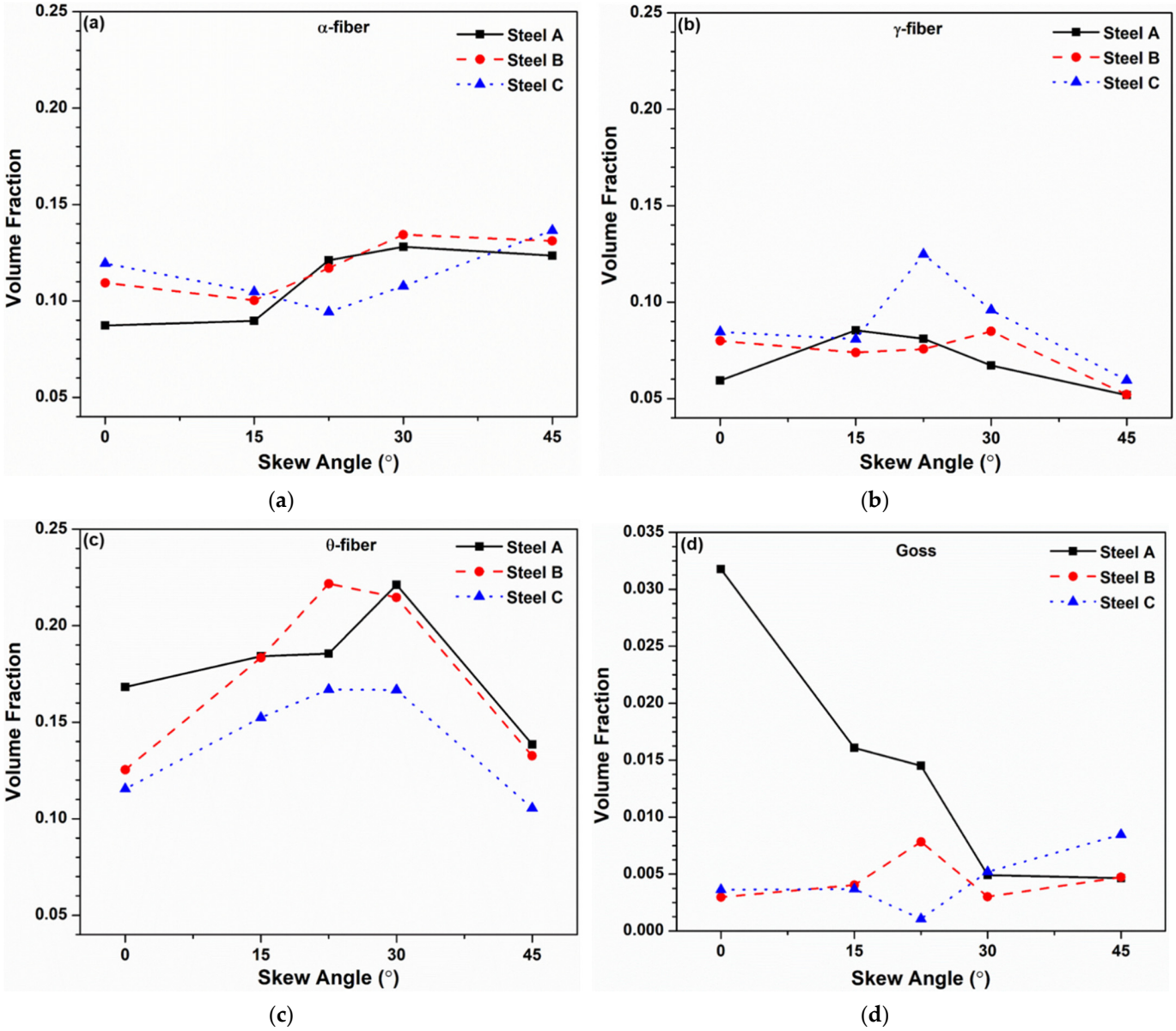

Figure 9. Variations of the volume fractions of common texture fibers, (**a**) α-fiber, (**b**) γ-fiber, (**c**) θ-fiber and the Goss component (**d**), after skew cold rolling and annealing (unidirectional feeding).

If the skew rolling angle is increased to 30°, a strong θ-fiber component {001}<120> is created in the 0.88% Si steel, while the γ-fiber is very weak (Figure 8a). These are also reflected in the volume fractions (Figure 9b,c). The Goss volume fraction of this steel continues to drop, while that of the α-fiber essentially does not change. The θ-fiber volume fractions of the 1.83% and 2.77% Si steels change only minimally, while the α-fiber volume fraction for both steels increases. The γ-fiber of the 2.77% Si steel drops considerably, while that of the 1.83% Si steel slightly increases.

When the skew angle is 45°, the extremely strong initial textures in the 0.88% and 1.83% Si steels are largely randomized, with the maximum texture intensities dropping from 31.55 to 3.56 and 38.04 to 8.35, respectively. Conversely, the 2.77% Si steel only shows a small decrease from 19.73 to 12.82. The θ-fiber and γ-fiber volume fractions of all the steels are considerably decreased, while the α-fiber is increased (2.77% Si steel) or essentially does not change (0.88% and 1.83% Si steels). The Goss component essentially does not change or slightly increases.

From the above analysis, it is observed that skew cold rolling (ω = 15°–30°) can considerably enhance the desired θ-fiber texture of all three steels after annealing, especially with respect to steels with relatively low silicon, i.e., Steels A and B. In most cases (except ω = 22.5° for the 2.77% Si steel), skew rolling will not change or only slightly increase (0.88% Si steel) the γ-fiber. However, skew rolling significantly weakens the Goss texture in the 0.88% Si steel, while only slightly affecting steels with higher silicon. Skew rolling at ω = 45° significantly decreases the θ-fiber and, thus, does not produce the desired texture.

3.3.2. Bidirectional Feeding

Annealing textures and volume fractions of typical fibers and the Goss component of the skew-cold-rolled steels are shown in Figures 10 and 11, respectively. As with *unidirectional feeding*, in most cases, the maximum texture intensities of the steels after annealing are significantly reduced. However, for the 2.77% Si steel after skew rolling at ω = 45°, the annealed material shows an extremely high intensity of 36.89 (near {332}<423>), which is much higher than the maximum intensity of this steel (23.05) after skew cold rolling, i.e., an almost single orientation is developed after annealing in this steel. Such a high texture intensity has also been reported in NOES after cross rolling [2].

At a 15° skew angle, the α-fiber is strengthened for all three steels, while the γ-fiber is essentially not affected. The θ-fiber of the 0.88% and 2.77% Si steels is weakened while that of the 1.83% Si steel increases considerably. Similarly to unidirectional feeding, the Goss component is essentially not affected by the 15° skew rolling for the 1.83% and 2.77% Si steels, but that of the 0.88% Si steel is significantly reduced.

When the skew angle increased to 22.5°, there is an apparent drop of the α-fiber for all three steels, as well as in the γ-fiber of the 1.83% and 2.77% Si steels. The γ-fiber of the 0.88% Si steel shows a slight increase at this skew angle. The θ-fiber of all three steels and the Goss component for the 1.83% and 2.77% Si steels all display an increase, whereas the Goss component of the 0.88% Si steel continues to drop, similar to what was observed with unidirectional feeding. The volume fractions of the Goss component of the 1.83% and 2.77% Si steels, on the other hand, show a large jump at this skew angle, especially the 2.77% Si steel.

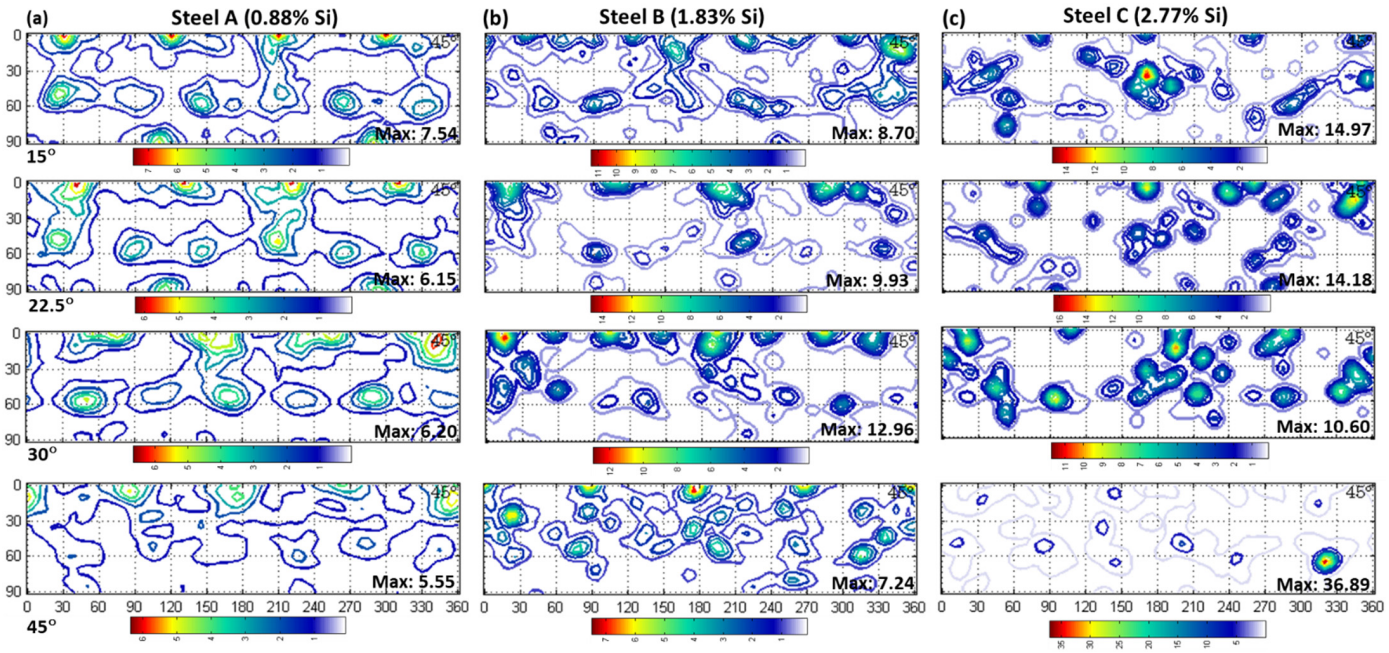

Figure 10. Textures of the skew-cold-rolled steels (bidirectional feeding) after annealing: (**a**) Steel A, (**b**) Steel B and (**c**) Steel C. φ_2 = 45° sections of the Euler space (Bunge notation).

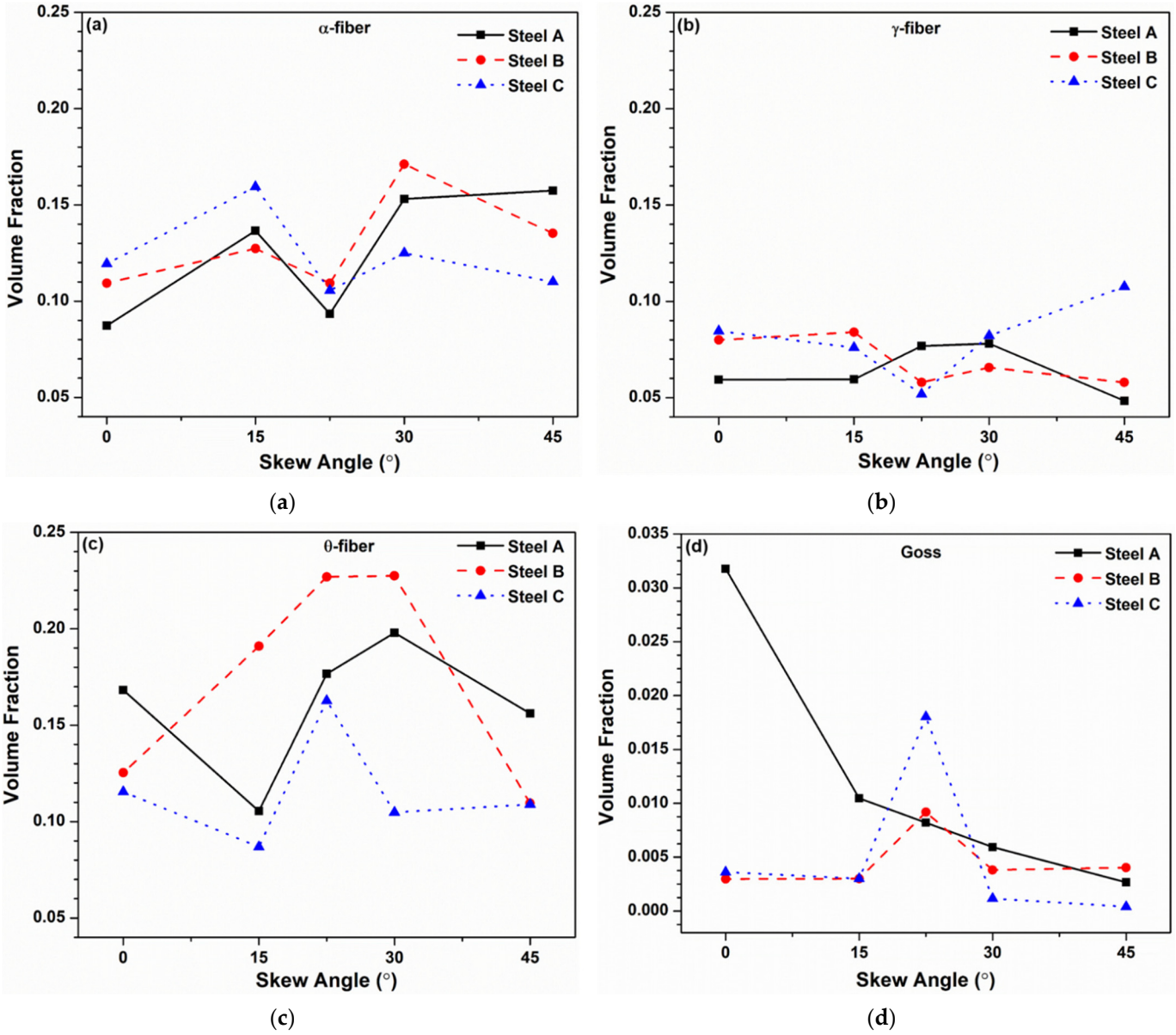

Figure 11. Variations of the volume fractions of common texture fibers, (**a**) α-fiber, (**b**) γ-fiber, (**c**) θ-fiber and the Goss component (**d**), after skew cold rolling and annealing (bidirectional feeding).

Increasing the skew angle to 30°, the volume fractions of the α-fiber for all the three steels increased again, while those of the γ-fiber are either slightly increased or do not change. The θ-fiber behaves differently for the three steels: The 0.88% Si steel increases, the 1.83% Si does not change and the 2.77% Si steel decreases. The Goss component shows a decrease for all three steels. When the skew angle increased to 45°, the volume fractions of all steels (except for the γ-fiber and θ-fiber of the 2.77% Si steel) decrease or essentially do not change. However, the increase in γ-fibers and θ-fibers of the 2.77% Si steel at this skew angle is very small.

Thus, for bidirectional feeding, skew rolling at an angle of 22.5° promotes the desired θ-fiber texture for all three steels, while for the 1.83% and 2.77% Si steels, the γ-fiber is also decreased to its lowest level, and Goss is considerably strengthened. Again, skew rolling at all angles decreases the Goss texture of the 0.88% Si steel when compared to conventional rolling.

3.3.3. Texture Factor

As mentioned before, the magnetic properties of non-oriented electrical steels are determined by a number of metallurgical factors, including grain size and texture. From a texture point of view, the θ-fiber (<001>//ND) texture should be maximized while the γ-fiber (<111>//ND) should be minimized to obtain optimal magnetic properties. In order to evaluate the magnetic quality of texture, the ratio of the volume fraction of the θ-fiber to that of the γ-fiber may be calculated, which reflects the overall quality of the texture of the material and is called "texture factor" by some authors [24,29]. Apparently, the larger the texture factor, the better the magnetic quality of the texture.

The variations of the texture factors of the steels after cold rolling and annealing are shown in Figure 12. Compared to conventional rolling (ω = 0°), skew rolling (ω > 0°) may or may not improve magnetic quality, depending on the Si content, the skew angle and the feeding scheme. For the low silicon steel (Steel A), at most angles, skew rolling decreases the texture factor; at angles that do increase the texture factor, i.e., 30° for unidirectional feeding and 45° for bidirectional feeding, the increase is very small (from ~2.8 to ~3.3). Thus, skew rolling may not be effective in improving the texture of low silicon steels. The effect of skew rolling on the texture factor of the high silicon steel (Steel C) is mostly small as well. However, at a skew angle of 22.5° under bidirectional feeding, there is a large increase in texture factor from 1.4 to 3.1. For the steel with 1.83 % Si (Steel B), the texture factor increased at all skew angles; at a skew angle of 22.5° (both unidirectional and bidirectional feeding), the texture factor increased the most, i.e., from 1.6 to 2.9 and 3.9, respectively.

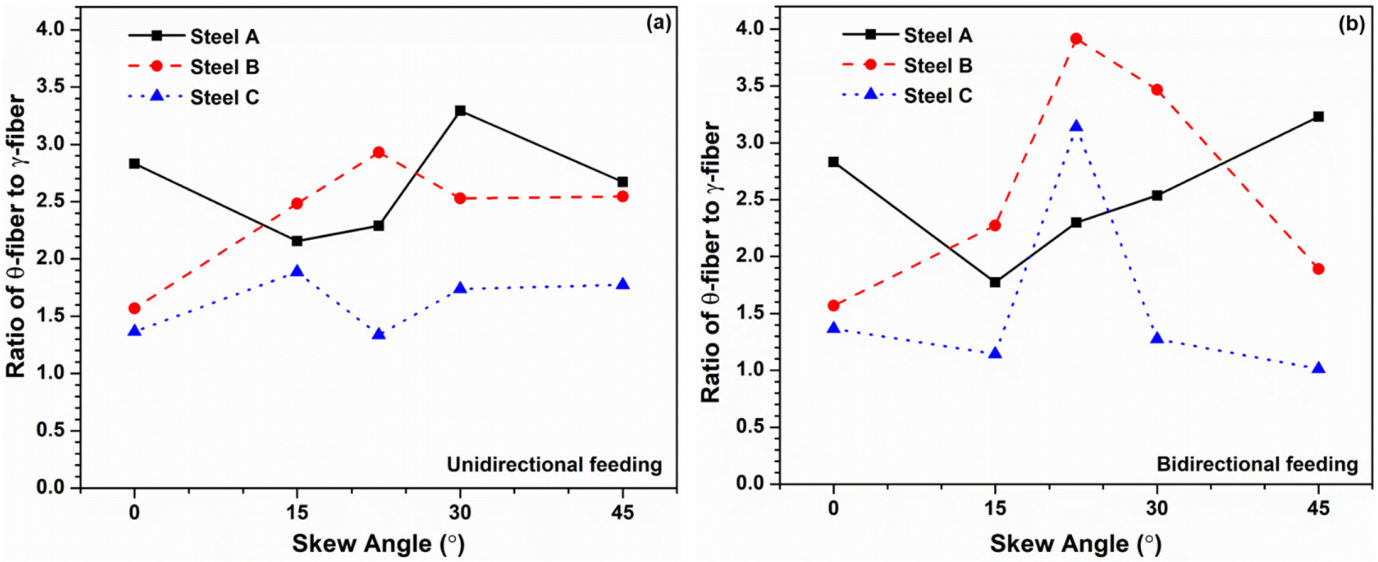

Figure 12. Effect of skew rolling angle on the texture factor (ratio of the θ-fiber to γ-fiber) of non-oriented electrical steels after annealing: (**a**) unidirectional feeding; (**b**) bidirectional feeding.

To summarize, skew rolling is most effective in improving the magnetic quality of the steel with 1.83% silicon (Steel B), and a skew angle of 22.5° increases the texture factor the most. However, it should be noted that the final texture of the electrical steel is also highly dependent on the annealing conditions applied to the cold-rolled material. The change of the annealing temperature, holding time and heating rate, etc., might result in significantly different final textures, which has yet to be further investigated.

4. Discussion

4.1. Deformation Texture

The crystallographic textures of metals after plastic deformation are determined by a number of factors [20,30], e.g., the crystal structure of the metal, the nature of the defor-

mation, the chemical composition, the deformation temperature, the initial texture, the deformation history of the material, etc. For NOES (BCC) during cold rolling, the dominant factors include the deformation mode and the initial texture. Since skew rolling uses samples cut from the same hot-rolled and annealed steel band, the starting materials have the same chemical composition, microstructure and processing history. The only difference is crystallographic texture (different rotations around ND). Due to the different skew angles, the deformation modes and magnitudes are also different, which may activate different slip systems during the deformation process. As a result, skew rolling may result in different textures than compared to conventional rolling. The above analysis has shown that, for the same starting material, skew rolling at different angles does indeed result in significantly different textures.

After conventional cold rolling, the textures of all three steels mainly consist of the α-fiber and the γ-fiber, since orientations between {001}<110> and {111}<110> (on α-fiber) as well as {111}<112> (on γ-fiber) are the stable orientations during plane strain compression [20,30]. A strong {112}<110>/{223}<110> orientation on the α-fiber is observed in all three steels, this being the theoretically stable orientation for plane-strain compression, as predicted by full-constraint Taylor model [31]. The textures of the 0.88% and 1.83% Si steels before cold rolling (Figure 2a,b) both contain strong <001>//ND components (e.g., near rotated cube and cube). It is known that in conventional rolling, the rotated cube is generally stable, and the components on the <001>//ND fiber tend to rotate (around ND) to the rotated cube orientation [17,32]; in fact, both steels present a strongly rotated cube texture after conventional rolling (Figure 4a,b). The 2.77% Si steel, conversely, only shows a weak <001>//ND texture before cold rolling (Figure 2c); thus, the rotated cube texture after conventional cold rolling is weak (Figure 4c). The strong {113}<361> component in the initial texture of the 2.77% Si steel does not seem to cause a significantly different cold rolling texture from the other two steels (which do not have such a texture before cold rolling).

Skew cold rolling promotes θ-fiber texture, i.e., the larger the skew angle (ω), the higher the volume fraction of the θ-fiber. This is true for all the steels and for both unidirectional and bidirectional feeding processes. However, the volume fraction of the rotated cube component is decreased by skew rolling, and generally the larger the skew angle, the smaller the rotated cube volume fraction (except for Steel C at a skew angle of 45°). This is opposite to conventional cold rolling where the rotated cube is at a stable final orientation and is normally strengthened after cold rolling. This is mainly because skew rolling is not a plane-strain compression process [26], and there is a large shear deformation in the material, which, together with the different initial textures, causes different rotation paths of the crystals from conventional rolling, resulting in different textures. This can be further confirmed by the fact that the volume fractions of the θ-fiber before cold rolling are essentially the same for all skew angles, but only conventional rolling rotates the θ-fiber components towards the rotated cube and greatly strengthens it, while skew rolling does not seem to rotate the θ-fiber towards this orientation, especially when the skew angle is greater than 30°.

Steel C shows somewhat different textures from Steels A and B mainly because of the different initial texture before cold rolling, which is caused by the high concentration of silicon in this steel. It is well known [21,22] that, if the silicon content is more than about 2.5 wt%, the electrical steel only has a single ferrite phase, and there is no phase transformation. The texture after hot rolling is, therefore, considerably different from steels that have phase transformation (with low silicon contents). The very high intensity (29.83) of the {112}<110>/{223}<110> components in Steel C after skew rolling at $\omega = 15°$ (Figure 4c) may be due to the relatively strong {112}<110>/{223}<110> components already existing in the initial texture after 15° rotation (Figure 2c). Skew rolling further strengthened these components. In fact, the {112}<110>/{223}<110> components are quite strong in almost all steels after skew rolling at all the angles (except 45°), indicating the high stability of these components even under skew rolling conditions. The extremely strong {001}<140>

component formed at ω = 45° for Steels A and B may be due to the following: i) a strong orientation near {001}<140> already existing in the material before skew rolling (the result of the 45° rotation around ND) and ii) the very large shear strain at this skew angle [26], which may have favored the formation of this orientation (or in other words, this orientation is stable under skew rolling at ω = 45°). Steel C, which does not have a strong near {001}<140> orientation before skew rolling, does not produce such a strong {001}<140> texture. However, this has to be further investigated using theoretical models, e.g., by using crystal plasticity simulations.

The textures after skew cold rolling with *bidirectional* feeding are quite similar to those with *unidirectional* feeding. The major difference is that, at ω = 45°, Steel A shows an extremely strong texture close (5° away) to cube ({001}<100>), while Steels B and C do not show such a strong texture (Figure 6), although the strongest components are also close to cube. Theoretically, bidirectional feeding of the strip during alterative rolling passes does not change the deformation mode, but it does change the initial orientations of the crystals with respect to the rolls. However, due to the symmetry of the rolls, the deformation of the crystals is not expected to be different from unidirectional feeding. Nevertheless, in practice, because of distortion and bending of the material after the previous passes, it is very difficult to maintain exactly the same skew angle for the next passes, i.e., possible variations from the nominal skew angles at each pass may have occurred, which may cause different final textures after rolling for several passes. The differences between the deformation textures of unidirectional and bidirectional feeding might result from this.

4.2. Recrystallization Texture

Although it has been extensively studied, the present understanding of how recrystallization textures develop from the deformed matrices during annealing is still very limited and mostly only qualitative [33]. This is because the final texture of the annealed material is determined both by the nucleation and grain growth of new crystals from a deformed matrix that contains heterogeneously distributed grains strained to different levels (even within a grain), which makes in situ investigation difficult. Neither the oriented nucleation nor the oriented growth theory can explain all the recrystallization textures [33]. The various substructures (e.g., shear bands, transition bands, microbands, deformation bands, etc.) generated during cold deformation render the understanding of the nucleation process even more difficult as these are usually the preferred nucleation sites. These structures are normally very small, and the direct observation of the nucleation from these fine substructures at high temperatures is extremely difficult.

Nevertheless, many studies have shown that for bcc metals, the prominent fibers (α and γ) developed in the cold rolling (plane strain compression) process are largely retained in recrystallized texture [30,33]. However, the recrystallization textures observed after skew rolling in the three electrical steels investigated in this study are quite different from the cold rolling textures, as none of the steels shows common fiber textures (either α or γ) after recrystallization. The very long period of holding (60 h at 840 °C) during hot band annealing might be one of the reasons. The grain sizes after hot band annealing are very large (up to ~550 μm) [5,24], which are favorable for shear banding during cold deformation [5,34,35]. It is known that shear bands are preferred nucleation sites during recrystallization. The more extensive the shear bandings, the greater the number of shear band promoted nuclei and, normally, the greater the number of new crystal orientations. As a result, the original deformation texture may be replaced by new orientations different from the cold-rolled orientations.

On the other hand, because of the long soak at a relatively high temperature, the sizes of precipitates (e.g., AlN, MnS, etc.) in the material are presumed to be large and the distribution is normally uniform throughout the matrix [36]. These coarse precipitates have less retarding effect on primary recrystallization during annealing than fine precipitates, which results in more rapid recrystallization than compared to steels without hot band annealing where precipitates have smaller sizes and tend to localize at grain boundaries.

The weakening or elimination of the γ-fiber texture in the three steels in this study is the result of hot band annealing applied before cold rolling, which has been reported to weaken the γ-fiber texture in ferrite after recrystallization [36].

The current understanding of the formation of a specific recrystallization texture from the cold deformed matrix of bcc metals is mostly based on the study of conventionally rolled material. For example, Goss texture is believed to be nucleated from the shear bands/microbands of deformed grains, especially those with {111}<112>, {111}<110> and {112}<110> orientations [23,37,38]. The high-angle misorientations (boundaries) between the Goss and the matrix grains are believed to promote the preferred growth of this grain orientation. It is generally accepted that recrystallized {111} grains originate from deformed {111} grains that contain higher stored energy than <110>//RD and <001>//ND grains after plane-strain compression [5,23,33,39]. However, the special deformation mode in skew rolling not only changed deformation texture but also altered stored energies in the deformed grains than compared to conventional rolling. For example, as illustrated in [5], the θ-fiber orientations (including cube and rotated cube) show higher Taylor factors (and higher stored energy) than the <111>//ND orientations during simple shear (skew rolling induces large shear [26]), which is opposite to conventional rolling where <111>//ND grains have higher Taylor factors (higher stored energy) than <001>//ND grains. During recrystallization, the preferred nucleation sites for Goss or {111} grains have been changed, and the nucleation and growth of such grains are suppressed by other orientations. The nucleation and growth of {001} grains, on the other hand, can be promoted from the change in stored energy by skew rolling. The strengthening of the θ-fiber textures with $\omega = 15^\circ$–30° in steels after skew rolling might have been caused by this. However, in order to clearly understand the mechanisms, detailed studies on the nucleation and grain growth processes during recrystallization using advanced characterization techniques, e.g., in situ EBSD [4], may be needed.

5. Conclusions

In this study, three non-oriented electrical steels containing different amounts of silicon were skew cold rolled and annealed to investigate the effect of deformation mode and initial texture on the cold rolling and recrystallization textures. The results can be summarized as follows.

Skew cold rolling at small skew angles (15°–22.5°) produces similar deformation textures to the textures of bcc metals after conventional rolling, i.e., with α-fibers and γ-fibers as the main textures. However, when the skew angle is large (30° and 45°), a very strong component on the θ-fiber (close to cube) developed, which is significantly different from the texture normally observed in conventional rolling. The intensity of this component reaches 48.6 in the low silicon steel skew cold rolled at an angle of 45°.

Compared to conventional rolling, skew cold rolling generally strengthens <001>//ND (θ-fiber) texture, and the larger the skew angle, the stronger the θ-fiber. Skew cold rolling only slightly changes (weakens or strengthens) the α-fibers and γ-fibers. The rotated cube component is mostly weakened by skew cold rolling and normally the larger the skew angle, the weaker the rotated cube component.

The differences in deformation texture after skew rolling from those after conventional rolling are attributed to the different initial textures before cold rolling (rotation around ND) and to the different deformation mode (e.g., strong shear strain) in the skew rolling process.

After annealing, the recrystallization texture is significantly randomized, and normally the larger the maximum intensity after skew cold rolling, the smaller the maximum intensity after annealing. Skew rolling at 15–30° generally promotes θ-fiber texture, while the γ-fiber texture may be slightly weakened or strengthened. The Goss texture (after annealing) of the low silicon steel is largely weakened by skew rolling, and the larger the skew angle, the weaker the Goss texture.

Skew rolling is most effective in improving the magnetic quality of the steel with 1.83% silicon (Steel B), and at a skew angle of 22.5°, the texture factor (the ratio of the θ-fiber to the γ-fiber) increased the most (1.8–2.4 times).

Author Contributions: Conceptualization, Y.H. and E.J.H.; methodology, Y.H. and E.J.H.; formal analysis, Y.H.; original draft preparation, Y.H.; review and edit, Y.H. and E.J.H. All authors have read and agreed to the published version of the manuscript.

Funding: This research was funded by Natural Resources Canada through the Program of Energy Research and Development (Project: CMAT-20-12).

Institutional Review Board Statement: Not applicable.

Informed Consent Statement: Not applicable.

Data Availability Statement: Not applicable.

Acknowledgments: Michael Attard, Darren Bibby and Raul Santos are acknowledged for cold rolling and annealing electrical steels. Victoria Jarvis, McMaster Analytical X-ray Diffraction Facility, McMaster University, is thanked for XRD texture measurements.

Conflicts of Interest: The authors declare no conflict of interest.

References

1. Park, J.T.; Szpunar, J.A. Evolution of recrystallization texture in nonoriented electrical steels. *Acta Mater.* **2003**, *51*, 3037–3051. [CrossRef]
2. Kestens, L.; Jacobs, J. Texture control during the manufacturing of non-oriented electrical steels. *Texture Stress Microstruct.* **2008**, *2008*, 173083. [CrossRef]
3. Sha, Y.H.; Sun, C.; Zhang, F.; Patel, D.; Chen, X.; Kalidindi, S.R.; Zuo, L. Strong cube recrystallization texture in silicon steel by twin-roll casting process. *Acta Mater.* **2014**, *76*, 106–117. [CrossRef]
4. Takajo, S.; Merriman, C.C.; Vogel, S.C.; Field, D.P. In-situ EBSD study on the cube texture evolution in 3 wt% si steel complemented by ex-situ EBSD experiment—From nucleation to grain growth. *Acta Mater.* **2019**, *166*, 100–112. [CrossRef]
5. Mehdi, M.; He, Y.; Hilinski, E.J.; Kestens, L.A.; Edrisy, A. The evolution of cube ({001}<100>) texture in non-oriented electrical steel. *Acta Mater.* **2020**, *185*, 540–554. [CrossRef]
6. Jiao, H.T.; Xu, Y.B.; Zhao, L.Z.; Misra, R.D.K.; Tang, Y.C.; Liu, D.J.; Hu, Y.; Zhao, M.J.; Shen, M.X. Texture evolution in twin-roll strip cast non-oriented electrical steel with strong Cube and Goss texture. *Acta Mater.* **2020**, *199*, 311–325. [CrossRef]
7. Wu, S.Y.; Lin, C.H.; Hsu, W.C.; Chang, L.; Sun, P.-L.; Kao, P.W. Effect of heating rate on the development of annealing texture in a 1.09 wt.% Si non-oriented electrical steel. *ISIJ Int.* **2016**, *56*, 326–334. [CrossRef]
8. Liang, R.; Yang, P.; Mao, W. Retaining {1 0 0} texture from initial columnar grains in 6.5 wt% Si electrical steels. *J. Magn. Magn. Mater.* **2017**, *411*, 511–516. [CrossRef]
9. Liu, H.T.; Schneider, J.; Li, H.L.; Sun, Y.; Gao, F.; Lu, H.H.; Song, H.Y.; Li, L.; Geng, D.Q.; Liu, Z.Y.; et al. Fabrication of high permeability non-oriented electrical steels by increasing <001> recrystallization texture using compacted strip casting processes. *J. Magn. Magn. Mater.* **2015**, *374*, 577–586. [CrossRef]
10. Ji, M.; Slater, C.; Davis, C. Thermomechanical Processing Map in Retaining {100}//ND texture via Strain-Induced Boundary Migration Recrystallization Mechanism. *Metall. Mater. Trans. A* **2020**, *51*, 6498–6504. [CrossRef]
11. Yasiki, H.; Kaneko, T. Effect of hot-band annealing on anisotropy of magnetic properties in low-Si semi-processed electrical steels. *J. Magn. Magn. Mater.* **1992**, *112*, 200–202. [CrossRef]
12. Lee, K.M.; Huh, M.Y.; Lee, H.J.; Park, J.T.; Kim, J.S.; Shin, E.J.; Engler, O. Effect of hot band grain size on development of textures and magnetic properties in 2.0% Si non-oriented electrical steel sheet. *J. Magn. Magn. Mater.* **2015**, *396*, 53–64. [CrossRef]
13. Wang, Y.Q.; Zhang, X.M.; Zu, G.Q.; Guan, Y.; Ji, G.F.; Misra, R.D.K. Effect of hot band annealing on microstructure, texture and magnetic properties of non-oriented electrical steel processed by twin-roll strip casting. *J. Magn. Magn. Mater.* **2018**, *460*, 41–53. [CrossRef]
14. De Campos, M.F.; Landgraf, F.J.G.; Takanohashi, R.; Chagas, F.C.; Falleiros, I.G.S.; Fronzaglia, G.C.; Kahn, H. Effect of the Hot Band Grain Size and Intermediate Annealing on the Deformation and Recrystallization Textures in Low Silicon Electrical Steels. *ISIJ Int.* **2004**, *44*, 591–597. [CrossRef]
15. Takashima, M.; Komatsubara, M.; Nobuyuki, M. {001} Texture Development by Two-stage Cold Rolling Method in Non-oriented Electrical Steel. *ISIJ Int.* **1997**, *37*, 1263–1268. [CrossRef]
16. Sonboli, A.; Toroghinejad, M.R.; Edris, H.; Szpunar, J.A. Effect of deformation route and intermediate annealing on magnetic anisotropy and magnetic properties of a 1wt% Si non-oriented electrical steel. *J. Magn. Magn. Mater.* **2015**, *385*, 331–338. [CrossRef]
17. Dillamore, I.L.; Roberts, W.T. Rolling textures in f.c.c. and b.c.c. metals. *Acta Metall.* **1964**, *12*, 281–293. [CrossRef]

18. Toth, L.; Jonas, J.; Daniel, D.; Ray, R. Development of ferrite rolling textures in low-and extra low-carbon steels. *Metall. Mater. Trans. A* **1990**, *21*, 2985–3000. [CrossRef]
19. Ray, R.; Jonas, J.J.; Hook, R. Cold rolling and annealing textures in low carbon and extra low carbon steels. *Int. Mater. Rev.* **1994**, *39*, 129–172. [CrossRef]
20. Raabe, D. Simulation of rolling textures of bcc metals considering grain interactions and crystallographic slip on {110},{112} and {123} planes. *Mater. Sci. Eng. A* **1995**, *197*, 31–37. [CrossRef]
21. Fischer, O.; Schneider, J. Influence of Deformation Process on the Improvement of Nonoriented Electrical Steel. *J. Magn. Magn. Mater.* **2003**, *254–255*, 302–306. [CrossRef]
22. Akta, S.; Richardson, G.J.; Sellars, C.M. Hot Deformation and Recrystallization of 3% Silicon: Steel Part 1: Microstructure, Flow Stress and Recrystallization Characteristics. *ISIJ Int.* **2005**, *45*, 1666–1675. [CrossRef]
23. Hayakawa, Y.; Kurosawa, M. Orientation relationship between primary and secondary recrystallized texture in electrical steel. *Acta Mater.* **2002**, *50*, 4527–4534. [CrossRef]
24. He, Y.; Hilinski, E.; Li, J. Texture Evolution of a Non-oriented Electrical Steel Cold Rolled at Directions Different from the Hot Rolling Direction. *Metall. Mater. Trans. A* **2015**, *46*, 5350–5365. [CrossRef]
25. Sidor, J.; Miroux, A.; Petrov, R.; Kestens, L. Microstructural and crystallographic aspects of conventional and asymmetric rolling processes. *Acta Mater.* **2008**, *56*, 2495–2507. [CrossRef]
26. He, Y.; Hilinski, E. Skew Rolling and Its Effect on the Deformation Texture of Non-oriented Electrical Steels. *J. Mater. Process. Technol.* **2017**, *242*, 182–195. [CrossRef]
27. Bohm, T.; Schneider, J.; Telger, K.; Wuppermann, C.D.; Kawalla, R.; Friedrich, K.E. Method of producing non-grain-oriented electrical sheet. U.S. Patent No. 6,582,528 B1, 24 June 2003.
28. Hielscher, R.; Schaeben, H. A novel pole figure inversion method: Specification of the MTEX algorithm. *J. Appl. Cryst.* **2008**, *41*, 1024–1037. [CrossRef]
29. Chang, S.K.; Huang, W.Y. Texture Effect on Magnetic Properties by Alloying Specific Elements in Non-grain Oriented Silicon Steels. *ISIJ Int.* **2005**, *45*, 918–922. [CrossRef]
30. Kestens, L.A.I.; Pirgazi, H. Texture formation in metal alloys with cubic crystal structures. *Mater. Sci. Technol.* **2016**, *32*, 1303–1315. [CrossRef]
31. Kestens, L.; Jonas, J.J. Transformation and Recrystallization Textures Associated with Steel Processing. In *ASM Handbook, Metalworking: Bulk Forming*; Semiatin, S.L., Ed.; ASM International: Materials Park, OH, USA, 2005; Volume 14A, pp. 685–700.
32. Xu, H.J.; Xu, Y.B.; He, Y.; Cheng, S.F.; Jiao, H.T.; Yue, S.; Li, J.P. Two-stage warm cross rolling and its effect on the microstructure, texture and magnetic properties of an Fe-6.5 wt% Si non-oriented electrical steel. *J. Mater. Sci.* **2020**, *55*, 12525–12543. [CrossRef]
33. Humphreys, F.J.; Hatherly, M. *Recrystallization and Related Annealing Phenomena*, 2nd ed.; Elsevier Ltd.: Oxford, UK, 2004; pp. 379–413.
34. Ridha, A.A.; Hutchinson, W.B. Recrystalllization mechanisms and the origin of cube texture in copper. *Acta Metall.* **1982**, *30*, 1929–1939. [CrossRef]
35. Korbel, A.; Embury, J.D.; Hatherly, M.; Martin, P.L.; Erbsloh, H.W. Microstructural aspects of strain localization in Al-Mg alloys. *Acta Metall.* **1986**, *34*, 1999–2009. [CrossRef]
36. Oliveira Malta, P.O.; Gonçalves, C.M.; Alves, D.S.; Ferreira, A.O.V.; Moutinho, I.D.; Santos, D.B. The influence of hot band annealing on recrystallization kinetics and texture evolution in a cold-rolled Nb-stabilized ferritic stainless steel during isothermal annealing. *J. Mater. Res.* **2016**, *31*, 2838–2849. [CrossRef]
37. Dorner, D.; Zaefferer, S.; Raabe, D. Retention of the Goss orientation between microbands during cold rolling of an Fe3% Si single crystal. *Acta Mater.* **2007**, *55*, 2519–2530. [CrossRef]
38. Mehdi, M.; He, Y.; Hilinski, E.J.; Kestens, L.A.I.; Edrisy, A. The Origins of the Goss Orientation in Non-Oriented Electrical Steel and the Evolution of the Goss Texture during Thermomechanical Processing. *Steel Res. Int.* **2019**, *80*, 1800582. [CrossRef]
39. Dillamore, I.; Roberts, W. Preferred orientation in wrought and annealed metals. *Metall. Rev.* **1965**, *10*, 271–380. [CrossRef]